Effect of 5d transition metals doping on the photocatalytic properties of rutile TiO_2

J. Belošević-Čavor*, V. Koteski, A. Umićević, V. Ivanovski

Institute of Nuclear Sciences Vinča, University of Belgrade, Belgrade, Serbia

Abstract

Density functional theory (DFT) calculations were performed to address the effects of 5d transition metals (TM) doping on the electronic structure properties of rutile TiO_2, using both the modified Becke-Johnson (mBJ) and on-site hybrid functional. The calculations show that there is a reduction of band gap in almost all the investigated cases, except when TiO_2 is doped with Ta. Some of the investigated systems (Re, W, Os, Ir) exhibit pronounced spin polarization, mainly arising from the TM atoms. In addition, a large increase of band gap is observed, when switching from a 24-atoms to 48-atoms supercell, while further enlarging the supercell size doesn't affect the band gap significantly. Among the investigated transition metals, Pt and Ir are the best candidates for improving the photocatalytic properties of rutile TiO_2 through substitutional doping.

Keywords: first principles calculations; TiO_2; transition metals; photocatalysis

1. Introduction

Titanium dioxide has proven to be the leading material for photocatalyst applications and as such has been extensively studied in both single, anatase and rutile, and mixed-phase form [1, 2]. Among other investigations transition metal doping of TiO_2 has received special interest due to potential applications including improved photocatalysis, solar energy production, and designing dilute magnetic semiconductors. Doping is an effective and easy method to adjust the TiO_2 band gap and extend the optical absorption edge toward the longer wavelengths, which increases its

*Corresponding author: e-mail cjeca@vinca.rs, fax +381-11-3408-681, phone +381-11-3408-549

efficiency in using the solar spectrum and improves its photocatalytic efficiency [3]. Extensive theoretical and experimental work has been carried out to study the doping effects of most of the 3d [4-16] and 4d transition metals [15-26] and lanthanides [27]. It was even shown that the improved visible light photocatalytic activity of the TiO_2 can be achieved through Ti^{3+} self-doping, mainly owing to the excitation of Ti^{3+} ions via 3d $\rightarrow$ 3d transitions from the gap state to the empty excited state above the Fermi level [1]. As far as the doping effects of 5d transition metals are concerned, the focus was mainly on anatase TiO_2 [15, 16, 19, 20, 21, 22, 24, 28-30], while the rutile phase was much less investigated [31-34]. Hao et al. demonstrated that W^{6+} as donor dopant in anatase TiO_2 introduces 5d unoccupied orbitals in the conduction band (CB) bottom and moves the CB edge downward, which can accelerate the electron injection process [30]. Zhang et al. found that in the anatase TiO_2 CB moves downward gradually with increasing the tungsten content from 0.1 % to 2 % and then stays almost unchanged with increasing the W content from 2 % to 5 % [22]. Rosario and Pereira showed that Pt ions could be incorporated into the TiO_2 lattice at low Pt content levels, which is followed by the conversion of small portion of anatase in the rutile phase and the enhancement of the photocatalytic activity [35]. Choi et al. reported that Pt and Cr doped TiO_2, with relatively high fraction of rutile, exhibited significantly enhanced photocatalytic activity [15]. Significant energy gap narrowing together with enhanced optical absorption has been experimentally achieved using 5d elements such as W [22] and Pt [15, 35, 36]. This paper presents a systematic study of the effect of 5d transition metals (Hf, Ta, W, Re, Os, Ir, Pt) doping on the photocatalytic properties of rutile TiO_2. We have performed an analysis to investigate the effects of these elements on geometry and electronic structure properties, such as band stucture, density of states and conduction band (CB) levels, i.e. to explore how the conduction band and valence band edges of TiO_2 are influenced by these

dopants and whether the doping introduces band gap states. Furthermore, we have made an attempt to correlate the obtained results in order to comment on the efficiency of these systems for visible light photocatalytic applications.

Due to the well-known shortcoming of the DFT in describing defects in metal oxides, hybrid DFT has become the approach of choice for a proper description of the band gaps of these systems. In the study conducted by Ju et al. [2] it was demonstrated that the HSE06 hybrid functional with the proper choice of a fraction of the screened Hartree – Fock (HF) potential, can yield the exact band gaps of anatase and rutile TiO_2. However, although the calculations with HSE06 exchange-correlation functional are faster in comparison to the others hybrid methods, they are still slower than the calculations with the Tran-Blaha modified Becke-Johnson (TB-mBJ) exchange potential [37, 38], whose computational cost is comparable to local density approximation (LDA) and generalized gradient approximation (GGA) potentials. Since the earlier testing of the TB-mBJ showed that this procedure mimics many-body results in satisfactory way [39, 40], we conducted our research using this method. In order to establish the consistency of the hybrid DFT and our approach, we also did calculations with on-site hybrid functional for the investigated probes, but only for the smallest 2 x 2 x 1 supercell.

2. Calculation details

We have performed self-consistent calculations by means of full potential linearized augmented plane waves (FP-LAPW) method implemented in the Wien2k package [41]. Firstly the lattice parameters and the atomic positions were fully optimized with the PBE-GGA [42] exchange-correlation functional until all components of the residual forces were smaller than 3 mRy/a.u. and after that, the Tran-Blaha modified Becke-Johnson (TB-mBJ) [38] exchange potential was used. In the case of hybrid calculations with onsite-exact-exchange, where the GGA exchange-

correlation was partly replaced by exact exchange, the atomic positions were optimized separately. To study the doping effect of 5d transition metals on the electronic structure of rutile TiO_2, we introduced a TM atom by substituing one Ti atom in the 2 x 2 x 1 (24-atom), 2 x 2 x 2 (48-atom), and 2 x 2 x 3 (72-atom) supercells of rutile, which led to different doping concentrations of 4.16, 2.08, and 1.39 at. %, respectively. No symmetry constraints were applied to the doped structures. All calculations were spin polarized in order to describe the magnetic effects correctly. The band structures were calculated along the path in the rutile Brillouin Zone (BZ) with the most high-symmetry points. The cut-off parameter $R_{mt}K_{max}$ for limiting the number of plane waves was set to 7.0, where R_{mt} is the smallest value of all atomic sphere radii and K_{max} is the largest reciprocal lattice vector used in the plane wave expansion.

The BZ integrations within the self-consistency cycles were performed via a tetrahedron method [43], using 18 k points in the irreducible wedge of the Brillouin zone (4 x 4 x 6 mesh) and the self-consistency was achieved by demanding the convergence of the integrated charge difference between the last two iterations to be smaller than 10^{-5} electron. The obtained optimized lattice constants, a = 4.635 Å and c = 2.978 Å, for pure rutile TiO_2, are in reasonable agreement with the experimental values (a = 4.594 Å and c = 2.959 Å) [44]. The structure parameter of rutile, which determines the position of O atom in the unit cell is u = 0.305.

3. Results and discussion

3.1. Geometry structure

In rutile TiO_2 each Ti atom is bonded to four nearest and two second nearest oxygen atoms, with slightly different bond lengths (1.949 vs. 1.980 Å). Our calculated Ti-O bond lengths with the nearest and second nearest oxygen atoms are 1.962 Å and 1.999 Å. Introducing dopants into the rutile TiO_2 crystal leads to a change in the atomic distances. To study the lattice deformation, the bond lengths in the doped rutile TiO_2 after geometry optimization are summarized in Table 1.

First of all, we can see that for each transition metal dopant the bond lengths in the different supercells are similar, namely the size of the supercell doesn't seem to affect the bond lengths notably. The most pronounced difference is observed for Pt atom, but it doesn't exceed 2%. Furthermore most of the doping atoms cause an enlargement of the atomic distances, that is to say the distances between the substituted TM atoms and their nearest O atom are larger in comparison to the Ti – O bond length in pure rutile. The only exception is W-doped rutile, which makes the W – O bonds shorter than the corresponding Ti – O bonds. Similar behaviour was observed in W doped anatase TiO_2 [30].

Table 1: The interatomic distances, given in Å, in 5d TM doped TiO_2 for different supercell sizes

	2 x 2 x 1 supercell	**2 x 2 x 2 supercell**	**2 x 2 x 3 supercell**
Hf – O	2.036	2.057	2.062
Ta – O	1.988	1.985	1.986
W – O	1.942	1.959	1.942
Re – O	1.980	1.990	1.987
Os – O	1.990	1.966	1.959
Ir – O	1.977	1.997	1.976
Pt – O	1.992	2.029	2.008

3.2. Defect formation energy

To investigate the relative difficulty of doping under different growth conditions, the doping formation energies for all studied cases were calculated using the formula:

$$E_f = E_d - E_p + \mu_X - \mu_{Ti}$$

where E_d and E_p are total energies of the supercells with and without dopants, respectively, μ_{Ti} is the chemical potential of Ti, and μ_X (X = Hf, Ta, Re, W, Os, Ir, Pt) is the chemical potential of dopants calculated from the bulk materials. Due to the fact that the chemical potential of Ti

varies with growth conditions, the formation energy also depends on them. Under the O-rich condition $\mu_{Ti} = \mu_{TiO2} - 2\ \mu_O$, where μ_O is half the total energy of the O_2 molecule. Under the Ti-rich condition, the Ti chemical potential is the energy of bulk Ti.

Table 2: Defect formation energies for different doped supercells

dopant	O-rich [eV]	Ti-rich [eV]
2 x 2 x 1		
Hf	-10.19	0.054
Ta	-10.38	-0.17
Re	-4.38	5.83
W	-7.85	2.39
Os	-4.56	5.69
Ir	-4.43	5.81
Pt	-1.80	8.44
2 x 2 x 2		
Hf	-9.49	0.72
Ta	-7.96	2.24
Re	-3.28	6.92
W	-5.51	4.70
Os	-1.72	8.48
Ir	-0.91	9.30
Pt	-0.56	9.65
2 x 2 x 3		
Hf	-7.66	2.58
Ta	-6.03	4.21
Re	-2.35	7.86
W	-3.52	6.72
Os	0.96	11.20
Ir	0.59	10.84
Pt	0.92	11.16

Our calculated formation energies for all investigated cases are summarized in Table 2, from which the following trends are observed: the doping is energetically more favorable under the O-rich than under the Ti-rich growth conditions; the systems with the lowest and second lowest formation energy are Hf and Ta doped ones, respectively, regardless of the growth conditions; Pt and Os are the most difficult to dope under both O-rich and Ti-rich growth conditions.

3.3. Band structure

To investigate the band structure modifications in the 5d TM doped rutile TiO_2, band structures for all the studied cases were calculated along the high-symmetry paths in the BZ. The obtained band structures for TM doped 2 x 2 x 2 rutile supercells are presented in figures 1 and 2. The calculated band structure of pure rutile TiO_2 (figure 1) is consistent with previous studies, showing a direct energy gap at the Γ point, with the energy gap value of 2.94 eV, which is similar to that calculated with HSE06 functional (2.92 eV [45]) and differs from the experimental value (3 eV [46]) by only 2%. Figures 1 and 2 demonstrate that all of the investigated systems display a direct energy gap at the Γ point and that almost all of them, except Ta, lead to band gap narrowing. In some cases (Re, W, Os, Ir) the existence of pronounced spin polarization is evident, i.e. the up and down spins are clearly different. The investigated systems can be divided into two groups: those for which the band gap narrowing is caused by the shift of the positions of the conduction band (CB) and valence band (VB) edges (Hf, Pt) and those with band gap narrowing as a consequence of formation of isolated intermediate states (IS) in the band gap region (Re, Os, Ir, W).

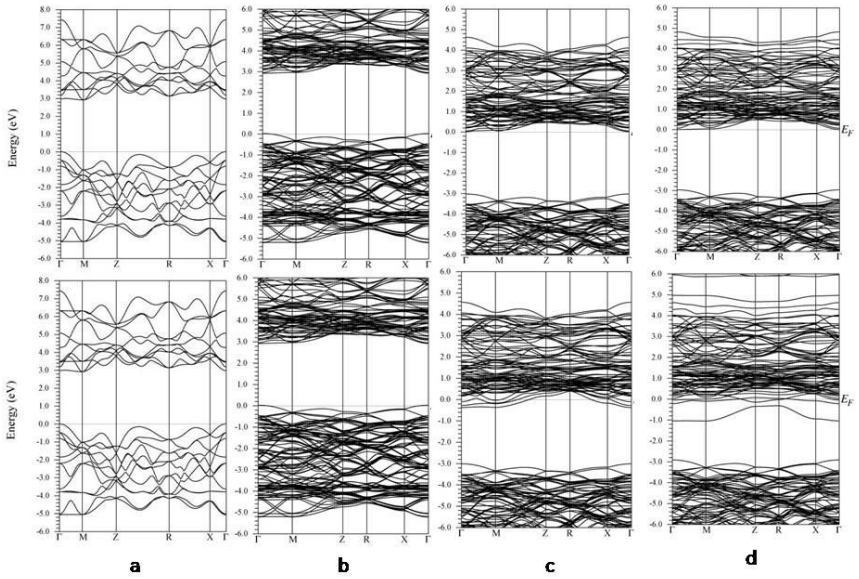

Figure 1: The mBJ calculated band structures of (a) pure and (b) Hf, (c) Ta and (d) W-doped rutile TiO_2 in 48-atoms supercell

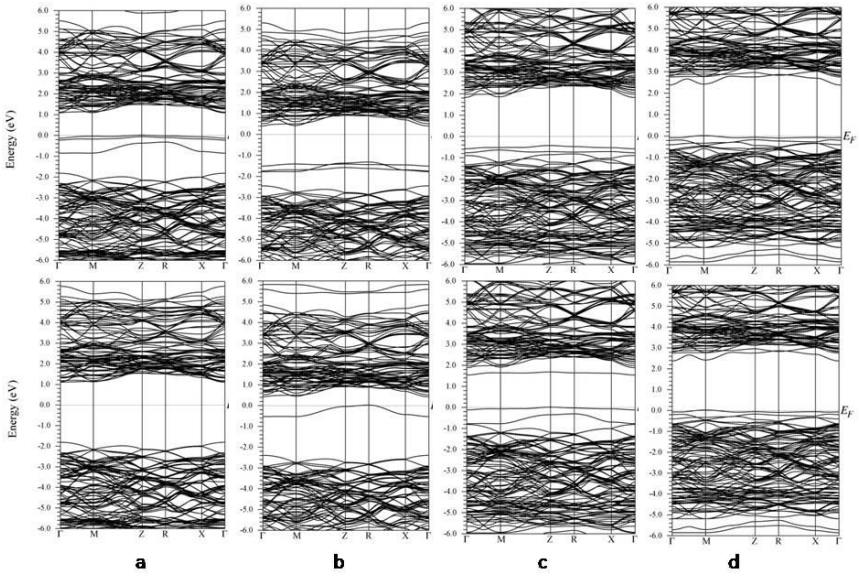

Figure 2: The mBJ calculated band structures of (a) Re, (b) Os and (c) Ir and (d) Pt-doped rutile TiO_2 in 48-atoms supercell

3.4. Density of states

To further understand the electronic structure of 5d TM doped TiO_2, the total densities of states (TDOS) and site-projected densities of states (PDOS) were calculated using 2 x 2 x 2 (48 atoms) rutile supercell. They are displayed in figures 3 and 4, with spin-up states plotted on the positive and spin-down states on the negative y-axes. It was found that the valence band of pure rutile is mostly composed of O 2p states, while in the conduction band Ti 3d states dominate. For Hf-doped TiO_2 the calculated band gap (table 3) and DOS are nearly identical to those of pure rutile TiO_2. The situation is similar for Ta-doped TiO_2, except for the fact that there is a small downward shift of the conduction band edge in the minority spin region and the Ta 5d states are spread over the whole CB. For the Re-doped TiO_2, the calculated DOS is more complex, as the up and down spins are evidently different, i. e. the DOS is notably spin-polarized.

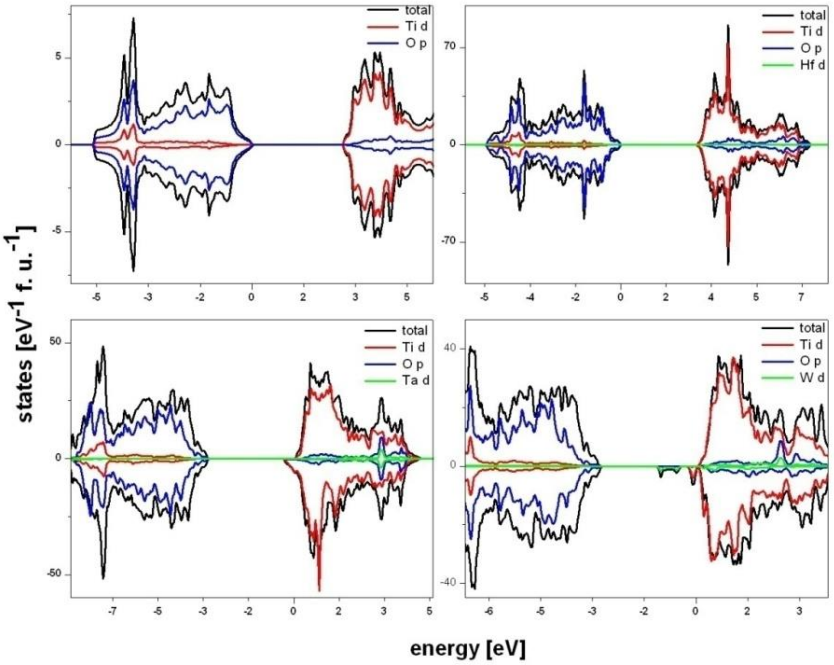

Figure 3: The mBJ calculated DOS for pure and Hf, Ta and W-doped rutile TiO_2 in 48-atoms supercell

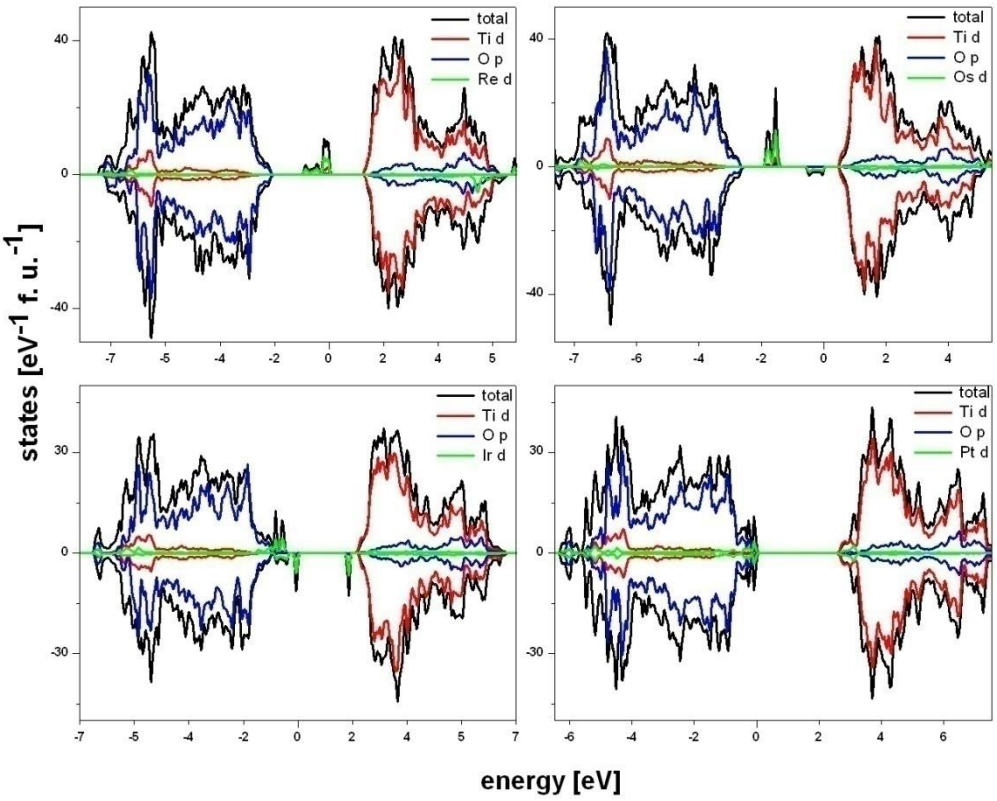

Figure 4: The mBJ calculated DOS for Re, Os, Ir and Pt-doped rutile TiO_2 in 48-atoms supercell

This observation is also confirmed by the calculated total spin magnetic moment in the unit cell (table 3), which is, unlike the Hf and Ta-doped rutile, significant. The total magnetic moment mainly arises from the Re atom, i. e. the spin-polarization occurs mainly at the Re site, but the calculations also indicate that the nearest neighbouring O and Ti atoms can be polarized up to 0.05 and-0.03 μ_B, respectively, due to the hybridization between the Re 5d states and the nearest neighbouring O 2p and Ti 3d states. From figure 4 we can see that doping rutile TiO_2 with Re atoms, leads to the creation of intermediate states, mostly Re 5d states, at the mid-band energy levels. In the case of W doped TiO_2 some W d states lie in the gap, near the conduction band

minimum (CBM), but only in the spin-down panel. Above them, at the CBM lie Ti d states. In total, the band gap is markedly narrowed in the spin-down panel. For the case of Os doping, several states, which originate mainly from the Os 5d electrons, appear in the band gap. The shape of the DOS is similar to that obtained in the earlier calculations, with the Fermi level which passes through the minority spin component, while the majority spin component remains semiconducting, which indicates that the system is half-metallic [32, 47]. Os 5d states in the majority spin channel are fully occupied and slightly splitted into two separate states, again similar as in the references [32, 47]. Spin polarization occurs mainly at the Os site, i. e. the total magnetic moment (2.0 μ_B) mainly arises from the magnetic moment of the Os atom (1.64 μ_B). Ir cation dopant introduces some impurity states at the top of the valence band, thus extending it into the band gap by about 0.5 eV. Furthermore, in the spin-down panel, two isolated Ir d states appear, one immediately above the valence band maximum (VBM) and the other under the CBM, which leads to different band gaps of the up- and down-energy bands. Pt doped rutile exhibits a large band gap contraction of about 0.71 eV, primarily due to the Pt d states at the top of the valence band, which causes the extension of the VB into the band gap.

Table 3: Band gaps and magnetic moments in 5d TM doped TiO_2 obtained from mBJ and on-site hybrid calculations

dopant	up gap - mBJ [eV]	down gap – mBJ [eV]	up gap - hibr [eV]	down gap – hibr [eV]	total magnetic moment in the cell – mBJ [μ_B]	TM magnetic moment – mBJ [μ_B]	total magnetic moment in the cell – hibr [μ_B]
2 x 2 x 1							
Hf	2.48	2.48	2.75	2.75	0	0	0
Ta	2.97	2.31	2.86	2.86	-1.0	-0.02	0
Re	2.80	2.86	0.76	2.58	3.0	2.25	3.0
W	1.44	1.69	1.74	1.74	1.0	0.08	-0.002
Os	1.41	1.58	1.66	1.60	2.0	1.76	2.0
Ir	1.39	0.22	2.28	0.03	1.0	0.66	1.0
Pt	1.28	1.28	2.31	2.31	0	0	0
2 x 2 x 2							
Hf	2.78	2.78			0	0	
Ta	2.97	2.53			-1.0	-0.01	
Re	2.78	2.80			3.0	2.16	
W	2.86	2.50			-1.97	-0.41	
Os	2.78	2.72			2.0	1.63	
Ir	2.12	1.77			1.0	0.81	
Pt	2.23	2.23			0	0	
2 x 2 x 3							
Hf	2.75	2.75			0	0	
Ta	2.86	2.56			-1.0	-0.01	
Re	2.75	2.78			3.0	2.20	
W	2.88	2.18			-2.0	-0.36	
Os	2.75	2.75			2.0	1.62	
Ir	2.23	2.48			1.0	0.79	
Pt	2.26	2.26			0	0	

3.5. Impact of doping concentration on the electronic structure

To investigate the influence of the doping concentration on the electronic structure, the DOS was also calculated for the systems with a TM atom in the 2 x 2 x 1 - 24 atoms (figure 5) and 2 x 2 x 3 - 72 atoms (figure 6) supercells of rutile, which corresponds to the TM content of 4.17 and 1.39 %, respectively. In some of the investigated cases (Hf, Ta, Re) there is no large difference in the DOS and band gap features for different sizes of supercells, aside from the fact that the intermediate bands in the smaller supercells are wider, making the energy gaps smaller. However, in the rest of the investigated systems (Os, W, Ir, Pt) a large increase of band gap occurs when switching from 2 x 2 x 1 to 2 x 2 x 2 supercell. Further increase of the supercell size to 2 x 2 x 3, doesn't seem to affect the band gaps significantly in any of the investigated cases, so we can conclude that the 2 x 2 x 2 supercell is large enough to avoid the interaction between the dopant atoms, which could lead to unrealistically small band gap values.

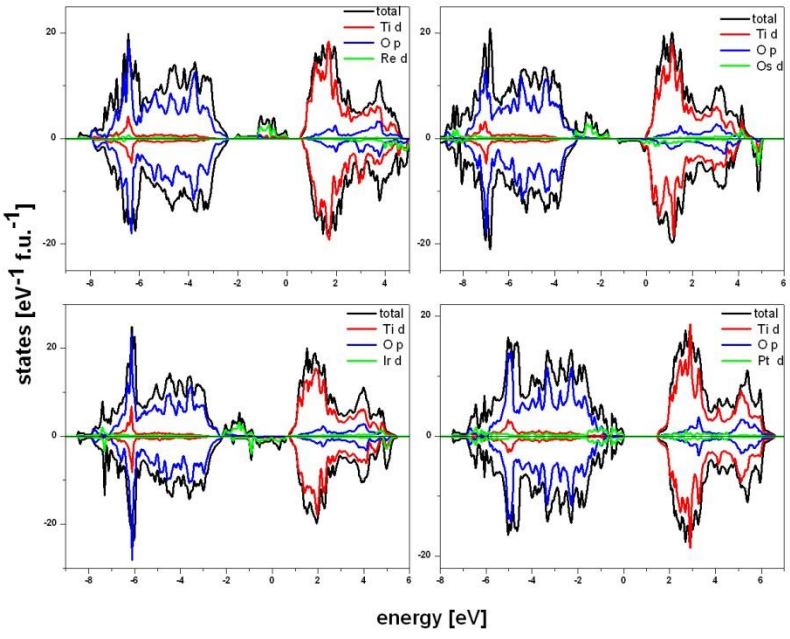

Figure 5: The mBJ calculated DOS for Re, Os, Ir and Pt-doped rutile TiO_2 in 24-atoms supercell

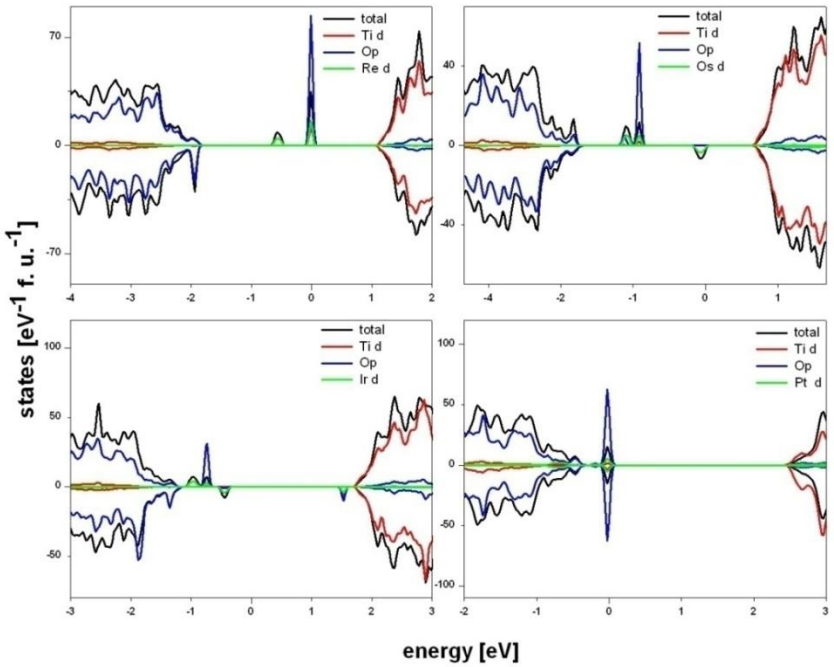

Figure 6: The mBJ calculated DOS for Re, Os, Ir and Pt-doped rutile TiO_2 in 72-atoms supercell

3.6. Bader analysis

To obtain more information on the charge distribution between the atoms, we employed the Bader's atoms in molecule theory [48], as implemented in the Critic2 code [49]. Bader's charge is defined as the difference between the electronic charge of the neutral atom and the electronic charge in the atomic basin of given atoms. The results of charge transfer analysis in the investigated systems are given in Table 4. We can see that TM atoms replace the Ti atom as a donor impurity in all studied cases and that the electron transfer from the Ti atom to O atom is reduced in comparison to that in pure TiO_2 on account of the transfer from TM to O atom. The amount of charge transferred from TM to O atom is mostly in accordance with their

electronegativity, that is to say the element with the largest electronegativity (Pt) has the smallest amount of charge transferred.

Table 4: Bader charges, in electrons, of Ti, O and TM atoms.

	Ti	O	TM
-	2.585	-1.292	
Hf	2.543	-1.362	3.009
Ta	2.531	-1.397	3.519
W	2.373	-1.348	3.522
Re	2.542	-1.283	2.768
Os	2.539	-1.282	2.479
Ir	2.557	-1.215	2.200
Pt	2.563	-1.234	1.955

3.7. Hybrid functional calculations

If we pay attention to the spin polarization and the magnetic moments in the cell, we see that two of the investigated TM stand out. Namely, Ta and W doped rutile, are the only systems that exhibit the spin polarized behaviour where the spin polarization doesn't occur mainly at the TM site. This may cast doubt on whether these systems are correctly described with the mBJ approximation. To clarify this dilemma and obtain more realistic picture of the electronic structure of the investigated materials, we also did calculations with onsite-exact-exchange, where the GGA exchange-correlation was partly replaced by exact exchange, but only for the simplest 2 x 2 x 1 supercell. The band gap values obtained in this way are also given in table 3 and the corresponding DOS plots are presented in figures 7 and 8.

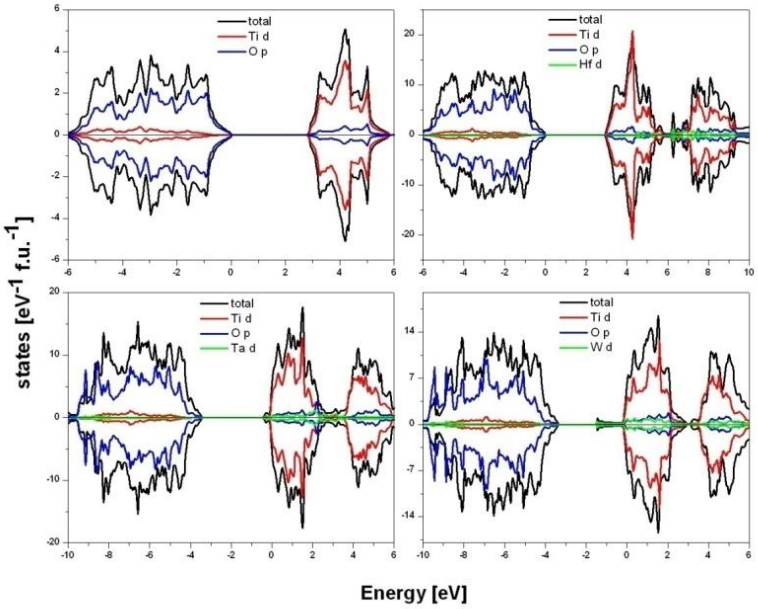

Figure 7: DOS for pure and Hf, Ta and W-doped rutile TiO_2 in 24-atoms supercell calculated with on-site hybrid functional

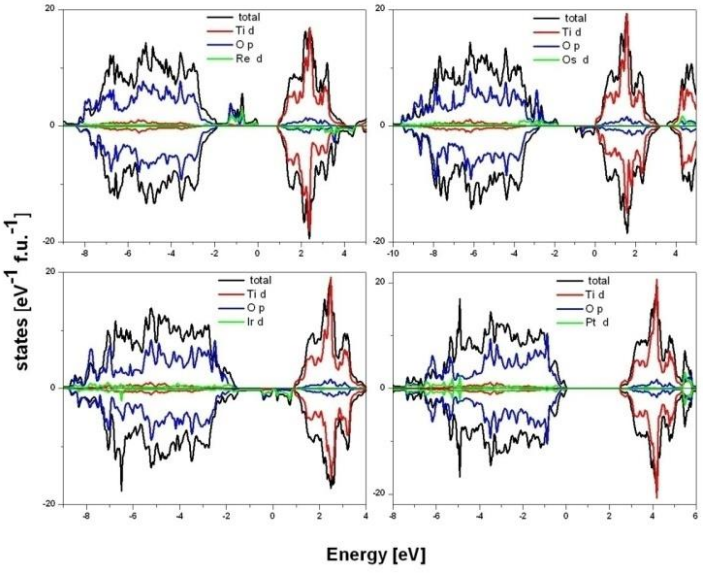

Figure 8: DOS for Re, Os, Ir and Pt-doped rutile TiO_2 in 24-atoms supercell calculated with on-site hybrid functional

The energy gap value for pure rutile TiO_2 obtained in this way is 2.81 eV. For Hf and Pt doped rutile, the overall profile of the total DOS obtained by hybrid potential is similar to that obtained by mBJ, except for a shift of the conduction bands to higher energy, which leads to a somewhat larger band gap. In the case of Re and Os doped rutile, the differences between the DOS plots obtained by hybrid and mBJ potentials are again small and mainly caused by the upward shift of the conduction bands. However the main difference in the DOS obtained by the two potentials is, as suspected, manifested for Ta and W doped rutile. Namely, the DOS obtained using the hybrid potential is not spin-polarized. The absence of spin polarization is also manifested in the total magnetic moments of the mentioned systems, which are almost zero. From figure 7 we can see that in both Ta and W doped rutile, the TM impurity atoms introduce TM d states at the bottom of the conduction band, which in the case of W streches into the band gap, resulting in its narrowing of about 40% as compared to that of pure rutile. Similar DOS, with the W 5d states just below CBM causing a band gap reduction, was obtained using the HSE06 functional [45]. However, in our case the decrease of the band gap is much larger, which is probably a consequence of the use of the 2 x 2 x 1 supercell instead of the 2 x 2 x 3 which was used in the HSE06 calculations, as it was demonstrated in the mBJ calculations that there is a large difference between the energy gap values for the 2 x 2 x 1 and 2 x 2 x 2 doped supercells. To further examine this discrepancy we performed hybrid functional calculations for W doped 2 x 2 x 2 supercell. Just as in the case of mBJ calculations, switching from 2 x 2 x 1 to 2 x 2 x 2 supercell has led to significant increase of band gap, whose value of 2.86 eV now compares much better with the one obtained using the HSE06 functional [45] and is similar to that obtained in our mBJ calculations. The increase of the supercell size also induced a small spin polarization in W-doped TiO_2 and the DOS shape is similar to that obtained from the mBJ calculations,

except for the fact that the W d states below the CBM are now moved further into the gap. The formation of W d states at the bottom of the conduction band was also observed in the W-doped anatase TiO_2 [30].

3.8. Optical absorption

The absorption spectra for all studied systems, plotted in figure 9, were calculated from the relation

$$\alpha(\omega) = \sqrt{2\left[\sqrt{\varepsilon_1{}^2(\omega) + \varepsilon_2{}^2(\omega)} - \varepsilon_1(\omega)\right]}$$

where $\alpha(\omega)$ is the absorption coefficient and $\varepsilon_1(\omega)$ and $\varepsilon_2(\omega)$ are the imaginary and the real part of the dielectric tensor. The imaginary part of the dielectric tensor $\varepsilon_1(\omega)$ for all the investigated systems was calculated from the computed band structure and then, the real parts of the dielectric tensor $\varepsilon_2(\omega)$ were evaluated using the Kramers-Kroning relation [50].

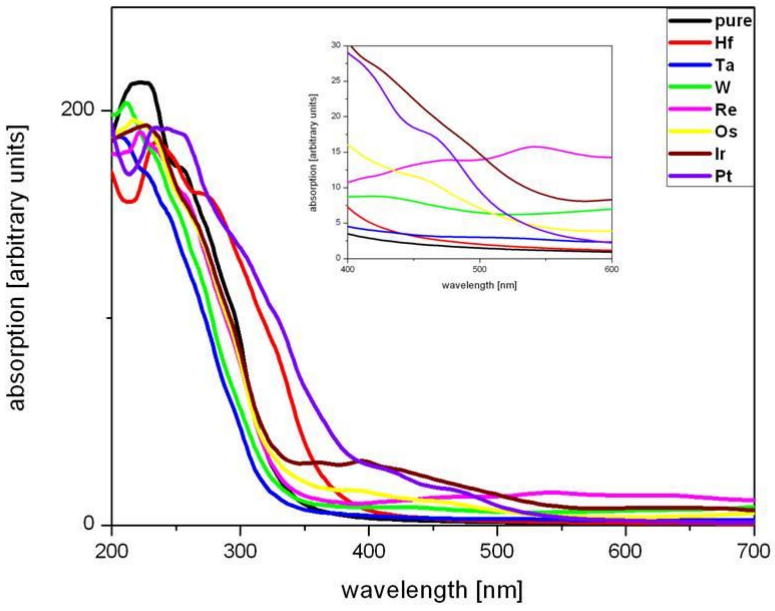

Figure 9: Optical absorption spectra of pure and TM doped TiO_2. The inserted segment represents the visible range.

As seen from figure 9, although the main absorption peaks for Pt and Hf doped rutile are red-shifted, they still occur in the UV range. However, the tails of the absorption edges extend up to the visible light region for most of the investigated dopants. Among them, Ir and Pt give the best visible light absorption, while Re has the longest extension of the absorption tail into the visible light region, probably due to the existence of the additional intraband transition between the Re d states in the gap and the Ti d states in the conduction band. The obtained absorption spectrum for Pt doped TiO_2 is consistent with the corresponding spectrum obtained from the UV-vis spectroscopic measurements [15], although the comparison is not straight forward, as the measured samples contained about 30% of rutile phase.

In order to evaluate the suitability of the investigated materials for visible light photocatalytic applications, we make an attempt to correlate our obtained results for electronic structure with the electronic structure that an efficient photocatalyst is supposed to have. To efficiently use rutile TiO_2 for photocatalytic water splitting, it is necessary to find a dopant which through the narrowing of the band gap, shifts the absorption edge to the visible light region, but at the same time does not lower the conduction band minimum, as the reduction potential level of water is just below the CBM of TiO_2 [51]. Furthermore, an efficient photocatalyst is supposed to have band gap with no additional states inside, which can act as electron-hole traps and recombination centers, reducing the lifetime of the photo-induced charge carriers and as a consequence also the photocatalytic activity. However, if the impurity states inside the gap do exist, they should be located in the lower or top third of the band gap, so the lifetime of the charge carriers will be reduced, but won't reach its minimum, as would do in the case these impurity states were created at the mid-band energy level. Taking all these criteria into account we can conclude that, among

the investigated transition metals, Pt and Ir, can be distinguished as the best candidates for improving the photocatalytic properties of rutile TiO_2 by doping.

4. Conclusion

In summary, using the first principles calculations, we have investigated the properties of interest for photocatalytic application, namely the band gap and absorption coefficients, in rutile TiO_2 substitutionaly doped with various 5d transition metals. In our investigation we have tested different supercell sizes and approximations for exchange-correlation potential. The calculated results indicate that all the investigated systems display a direct energy gap at the Γ point and that almost all of them, except Ta, in one way or another lead to band gap narrowing. Furthermore, it was found that a 2 x 2 x 1 supercell is not adequate for the realistic description of the investigated systems and that in order to get satisfying results 2 x 2 x 2 supercell must be used. The overall trend in the band gap changes is the same for the DOS obtained by mBJ and hybrid calculations. Taking all the criteria for the efficient photocatalyst for water splitting into account, we can conclude that among the investigated transition metals, Pt and Ir are the best candidates for improving rutile TiO_2 properties.

Acknowledgement

The financial support for this study was provided through the Project No. III 45018, financed by The Ministry of Education, Science and Technological Development of the Republic of Serbia.

Data availability

The raw/processed data required to reproduce these findings cannot be shared at this time due to technical limitations.

References

[1] Zhiqiang Wang, Bo Wen, Qunqing Hao, Li-Min Liu, Chuanyao Zhou, Xinchun Mao, Xiufeng Lang, Wen-Jin Yin, Dongxu Dai, Annabella Selloni and Xueming Yang, Localized Excitation of Ti^{3+} Ions in the Photoabsorption abd Photocatalytic Activity of Reduced Rutile TiO_2, Journal of the American Chemical Society 137 (2015) 9146-9152.

[2] Ming-Gang Ju, Guangxu Sun, Jiajun Wang, Qiangqiang Meng, and WanZhen Liang, Origin of High Photocatalytic Properties in the Mixed-Phase TiO_2: A First-Principles Theoretical Study, Applied Materials and Interfaces 6 (2014) 12885-12892.

[3] Mingzheng Ge, Jingsheng Cai, James Iocozzia, Chunyan Cao, Jianying Huang, Xinnan Zhang, Jiali Shen, Shanchi Wang, Songnan Zhang, Ke-Qin Zhang, Yuekun Lai, Zhiqun Lin, A review of TiO_2 nanostructured catalysts for sustainable H_2 generation, International Journal of Hydrogen Energy 42 (2017) 8418-8449.

[4] X. Li, J. Shi, H. Chen, R. Wan, C. Leng, S. Chen, Y. Lei, A DFT study on the modification mechanism of (Cr, C) co-doping for the electronic and optical properties of anatase TiO_2, Computational Materials Science 129 (2017) 295-303.

[5] R. Long, N. J. English, First-principles calculation of electronic structure of V-doped anatase TiO_2, Chem Phys Chem 11 (2010) 2606-2611.

[6] Fengzhu Ren, Haiyan Li, Yuanxu Wang, Jianjun Yang, Enhanced photocatalytic oxidation of propylene over V-doped TiO_2 photocatalyst: Reaction mechanism between V^{5+} and single-electron-trapped oxygen vacancy, Applied Catalysis B: Environmental 176 (2015) 160-172.

[7] G. Shao, Electronic Structures of Manganese-Doped Rutile TiO_2 from First Principles Journal of Physical Chemistry C 112 (2008) 18677-18685.

[8] G. Y. Gao, K. L. Yao, Z. L. Liu, J. Zhang, X. L. Li, J. Q. Zhang, N. Liu, Magnetism and electronic structure of Cr-doped rutile TiO_2 from first-principles calculations, Journal of Magnetism and Magnetic Materials 313 (2007) 210-213.

[9] W. T. Geng, Kwang S. Kim, Structural, electronic, and magnetic properties of a ferromagnetic semiconductor: Co-doped TiO_2 rutile, Physical Review B 68 (2003) 125203.

[10] Tsutomu Umebayashi, Tetsuya Yamaki, Hisayoshi Itoh, Keisuke Asai, Analysis of electronic structures of 3d transition metal-doped TiO_2 based on band calculations, Journal of Physics and Chemistry of Solids 63 (2002) 1909-1920.

[11] M. Saini, M. Kumar, T. Som, ab initio study of 3d transition metal-doping effects in rutile-TiO_2: Role of bandgap tunability in conductivity behaviour, Applied Surface Science 418 (2017) 302-307.

[12] Vejsel Çelik, Ersen Mete, Electronic and optical properties of Cr and Cr-N doped anatase TiO_2 from screened Coulomb hybrid calculations, J. Phys. Condens. Matter 25 (2013) 365502.

[13] Hongming Weng, Xiaoping Yang, Jinming Dong, H. Mizuseki, M. Kawasaki, Y. Kawazoe, Electronic structure and optical properties of the Co-doped anatase TiO_2 studied from first principles, Phys. Rev. B 69 (2004) 125219.

[14] Min Sik Park, S. K. Kwon, B. I. Min, Electronic structures of doped anatase TiO_2: $Ti_{1-x}M_xO_2$ (M = Co, Mn, Fe, Ni), Phys. Rev. B 65 (2002) 161201(R).

[15] Jina Choi, Hyunwoong Park, Michael R. Hoffmann, Effects of Single Metal-Ion Doping on the Visible-Light Photoreactivity of TiO_2, Journal of Physical Chemistry C 114 (2010) 783-792.

[16] J. W. Pan, C. Li, Y. F. Zhao, R. X. Liu, Y. Y. Gong, L. Y. Niu, X. J. Liu, B. Q. Chi, Electronic properties of TiO_2 doped with Sc, Y, La, Zr, Hf, V, Nb and Ta, Chemical Physics Letters 628 (2015) 43-48.

[17] Wolfgang Körner, Christian Elsässer, Density functional theory study of dopants in polycrystalline TiO_2, Physical Review B 83 (2011) 205315.

[18] Xiaohui Yu, Changsheng Li, Yun Ling, Ting-Ao Tang, Qiong Wu, Junjie Kong, First principles calculations of electronic and optical properties of Mo-doped rutile TiO_2, Journal of Alloys and Compounds 507 (2010) 33-37.

[19] K. E. Rammutla, S. L. P. Savin, M. G. Matshaba, A. V. Chadwick, P. E. Ngoepe, Studies of the location of precious metals in nanocrystalline titanium dioxide using XRD and XANES, phys. Stat. sol. (c) 4 (2007) 765-769.

[20] Benjamin J. Morgan, David O Scanlon, Graeme W. Watson, Small polarons in Nb- and Ta-doped rutile and anatase TiO_2, Journal of Materials Chemistry 19 (2009) 5175-5178.

[21] D. M. Tobaldi, R. C. Pullar, A. F. Gualtieri, M. P Seabra, J. A. Labrincha, Phase composition, crystal structure and microstructure of silver and tungsten doped TiO_2 nanopowders with tuneable photochromic behaviour, Acta Materialia 61 (2013) 5571-5585.

[22] Xi Zhang, Fang Liu, Qiu-Liu Huang, Gang Zhou, Zhong-Sheng Wang, Dye-Sensitized W-Doped TiO_2 Solar Cells with a Tunable Conduction Band and Suppressed Charge Recombination, The Journal of Physical Chemistry C 115 (2011) 12665-12671.

[23] Kenan Song, Xiaoping Han, Guosheng Shao, Electronic properties of rutile TiO_2 doped with 4d transition metals: First-principles study, Journal of Alloys and Compounds 551 (2013) 118-124.

[24] Kesong Yang, Ying Dai, Baibiao Huang, Yuan Ping Feng, First-principles GGA + U study of the different conducting properties in pentavalent-ion-doped anatase and rutile TiO_2, J. Phys. D: Appl. Phys. 47 (2014) 275101.

[25] Matiullah Khan, Wenbin Cao, Ning Chen, Zahid Usman, Dil Faraz Khan, Arbab Mohammad Toufiq, Murad Ali Khaskheli, Ifluence of tungsten doping concentration on the electronic and optical properties of anatase TiO_2, Current Applied Physics 13 (2013) 1376-1382.

[26] Yu-Chao Xia, Rui-Sheng Feng, Chuan-Sheng Wu, First-Principles Study on Band Structure of M-Doped TiO_2 (M = Ag, Co, Cr, Mn, Sb, Zn), Journal of Nanoelectronics and Optoelectronics 12 (2017) 1181-1185.

[27] Yanming Lin, Yunlong Su, Yanhua Zhu, Zhenyi Jiang, Hailong Shi, Xu Ding, Xiaodong Zhang, Haiyan Zhu, Ruiqin Zhang, The electronic structure and optical absorption of rutile TiO_2 with La and N dopants from first-principles calculation, Computational Materials Science 131 (2017) 178-186.

[28] R. Long, N. J. English, Tailoring the electronic structure of TiO2 by cation codoping from hybrid density functional theory calculations, Phys. Rev. B 83 (2011) 155209.

[29] R. Long, N. J. English, Electronic structure of cation-codoped TiO2 for visible-light photocatalyst applications from hybrid density functional theory calculations, Applied Physics Letters 98 (2011) 142103.

[30] Li Hao, Fu-Quan Bai, Chui-Peng Kong, Shamsa Bibi, Hong-Xing Zhang, Theoretical studies of heteroatom-doping in TiO_2 to enhance the electron injection in dye-sensitized solar cells, RSC Advances 5 (2015) 79868-79873.

[31] Y. Murata, S. Fukuta, S. Ishikawa, S. Yokoyama, Photoelectrochemical properties of TiO_2 rutile microalloyed with 4d and 5d transition elements, Solar Energy Materials and Solar Cells 62 (2000) 157-165.

[32] A. Fakhim Lamrani, M. Ouchri, M. Belaiche, A. El Kenz, M. Loulidi, A. Benyoussef, Half metallic antiferromagnetic behaviour in doped TiO_2 rutile with double impurities (Os, Mo) from ab initio calculations, Thin Solid Films 570 (2014) 45-48.

[33] X. Yu, C. Li, H. Tang, Y. Ling, T.-A. Tang, Q. Wu, J. Kong, First principles study on electronic structures and properties of Sn-doped rutile TiO_2, Computational Materials Science 49 (2010) 430-434.

[34] Prafulla K. Jha, Sanjeev K. Gupta, Igor Lukačević, Electronic structure, photocatalytic properties and phonon dispersions of X-doped (X = N, B and Pt) rutile TiO_2 from density functional theory, Solid State Sciences 22 (2013) 8-15.

[35] Adriane V. Rosario, Ernesto C. Pereira, The role of Pt addition on the photocatalytic activity of TiO_2 nanoparticles: The limit between doping and metallization, Applied Catalysis B: Environmental 144 (2014) 840-845.

[36] Kazuhiko Maeda, Photocatalytic properties of rutile TiO_2 powder for overall water splitting, Catalysis Science and Technology 4 (2014) 1949-1953.

[37] A. D. Becke and E. R. Johnson, A simple effective potential for exchange, J. Chem. Phys. 124 (2006) 221101.

[38] F. Tran, P. Blaha, Accurate Band Gaps of Semiconductors and Insulators with a Semilocal Exchange-Correlation Potential, Phys. Rev. Lett. 102 (2009) 226401.

[39] R. Armiento, S. Kummel, T. Korzdorfer, Electrical response of molecular chains in density functional theory: Ultranonlocal response from a semilocal functional, Phys. Rev. B 77 (2008) 165106.

[40] David J. Singh, Electronic structure calculations with the Tran-Blaha modified Becke-Johnson density functional, Physical Review B 82 (2010) 205102.

[41] P. Blaha, K. Schwarz, G. K. H. Madsen, D. Kvasnicka, J. Luitz, WIEN 2k an Augmented Plane Wave Plus Local Orbitals Program for Calculating Crystal Properties, Vienna University of Technology, Vienna, Austria, 2001.

[42] J. P. Perdew, K. Burke, M. Ernzerhof, Generalized Gradient Approximation Made Simple, Physical Review Letters 77 (1996) 3865-3868.

[43] P. E. Blochl, O. Jepsen, O. K. Andersen, Improved tetrahedron method for Brillouin-zone integrations, Physical Review B 49 (1994) 16223-16233.

[44] C. J. Howard, T. M. Sabine, F. Dickson, Structural and thermal parameters for rutile and anatase, Acta Crystallogr. B: Struct. Sci. 47 (1991) 462-468.

[45] H. Choi, S. Khan, J. Choi, D. T. T. Dinh, S. Y. Lee, U. Paik, S-H. Cho, S. Kim, Synergetic control of band gap and structural transformation for optimizing TiO_2 photocatalysts, Applied Catalysis B: Environmental 210 (2017) 513-521.

[46] A. Amtout, R. Leonelli, Optical properties of rutile near its fundamental band gap, Physical Review B 51 (1995) 6842-6851.

[47] A. Fakhim Lamrani, M. Ouchri, M. Belaiche, A. El Kenz, M. Loulidi, A. Benyoussef, The effect of fluorine doping on electronic structure and ferromagnetic stability of Os-doped TiO_2 rutile phase: First-principles calculations, Journal of Magnetism and Magnetic Materials 401 (2016) 977-981.

[48] R. F. W. Bader, Atoms in Molecules: A Quantum Theory, Oxford University Press, Oxford, 1990.

[49] A. O. de-la Roza, E. R. Johnson, V. Luana, Critic2: a program for real-space analysis of quantum chemical interactions in solids, Comput. Phys. Commun. 185 (3) (2014) 1007–1018.

[50] D. B. Melrose, R. J. Stoneham, Generalised Kramers-Kronig formula for spatially dispersive media, J. Phys. A: Math. Gen. 10 (1977) L17.

[51] K. Maeda, K. Domen, New Non-Oxide Photocatalysts Designed for Overall Water Splitting under Visible Light, J. Phys. Chem. C 111 (2007) 7851-7861.